International Journal of Remote Sensing
Vol. 30, No. 13, 10 July 2009, 3463–3483

Taylor & Francis
Taylor & Francis Group

An empirical study on the utility of BRDF model parameters and topographic parameters for mapping vegetation in a semi-arid region with MISR imagery

LIHONG SU*†, YUXIA HUANG‡, M. J. CHOPPING§, A. RANGO¶ and J. V. MARTONCHIK††

†University of North Carolina at Chapel Hill, Department of Geography, Chapel Hill, NC 27599, USA

‡Department of Computing Sciences, Texas A&M University, Corpus Christi, TX 78412, USA

§Montclair State University, Department of Earth and Environmental Studies, Montclair, NJ 07043, USA

¶USDA, ARS Jornada Experimental Range, Las Cruces, NM 88003, USA

††NASA Jet Propulsion Laboratory, Pasadena, CA 91109, USA

(*Received 6 November 2007; in final form 26 May 2008*)

In this study we show that multiangle remote sensing is useful for increasing the accuracy of vegetation community type mapping in desert regions. Using images from the National Aeronautics and Space Administration (NASA) Multiangle Imaging Spectroradiometer (MISR), we compared roles played by Bidirectional Reflectance Distribution Function (BRDF) model parameters with those played by topographic parameters in improving vegetation community type classifications for the Jornada Experimental Range and the Sevilleta National Wildlife Refuge in New Mexico, USA. The BRDF models used were the Rahman–Pinty–Verstraete (RPV) model and the RossThin-LiSparseReciprocal (RTnLS) model. MISR nadir multispectral reflectance was considered as baseline because nadir observation is the most basic remote sensing observation. The BRDF model parameters and the topographic parameters were considered as additional data. The BRDF model parameters were obtained by inversion of the RPV model and the RTnLS model against the MISR multiangle reflectance data. The results of 32 classification experiments show that the BRDF model parameters are useful for vegetation mapping; they can be used to raise classification accuracies by providing information that is not available in the spectral-nadir domain, or from ancillary topographic parameters. This study suggests that the Moderate Resolution Imaging Spectroradiometer (MODIS) and MISR BRDF model parameter data products have great potential to be used as additional information for vegetation mapping.

1. Introduction

Vegetation mapping in a semi-arid region is a classification problem in which the classes are the recognized plant community types (Kremer and Running 1993). A plant community type may be defined as an aggregation of plant types that demonstrate mutual inter-relationships between species and between species and the

*Corresponding author. Email: sul@email.unc.edu

International Journal of Remote Sensing
ISSN 0143-1161 print/ISSN 1366-5901 online
http://www.tandf.co.uk/journals
DOI: 10.1080/01431160802562230

environment. Usually, community type differentiation implies a larger number of classes that differ more subtly than the broader categories assigned to regional or global classification schemes (Chopping *et al.* 2002). Mapping semi-arid vegetation types at the community level is challenging (Loveland *et al.* 2000, Langley *et al.* 2001, Chopping *et al.* 2002, Akbari *et al.* 2006). The ability of the Multiangle Imaging Spectroradiometer (MISR) to obtain quasi-simultaneous multispectral measurements at nine view angles allowed information to be collected for quantifying canopy structure and photosynthetic activity, and also for mapping vegetation (Diner *et al.* 1999, 2005, Gobron *et al.* 2000, Zhang *et al.* 2002, Nolin 2004). Multiple view angle observations have also proved to be useful for improving classification accuracy of land cover classes (Kimes *et al.* 1991, Abuelgasim *et al.* 1996, Sandmeier and Deering 1999, Chopping *et al.* 2002, Xavier and Galvão 2005, Armston *et al.* 2007, Liesenberg *et al.* 2007, Su *et al.* 2007*a*,*b*).

All surfaces, both natural and man-made, show some degree of spectral reflectance anisotropy when illuminated by sunlight. The anisotropic behaviour of surface reflectance is described by the Bidirectional Reflectance Distribution Function (BRDF). BRDF shapes of vegetated surfaces are largely determined by density, geometry and the spatial distribution of crowns at the scene level of a sensor's footprint (Li and Strahler 1992). Structural characteristics at the canopy level, such as the leaf area index, leaf angle distribution and foliage clumping, also play a major role (Ross 1981, Myneni and Asrar 1993, Chen and Cihlar 1995). BRDF models link spectral properties of components and the structure of canopy–soil complexes in a remote sensing pixel with sensor-measured radiance. A number of BRDF models have been proposed in the literature (Asner 2000, Liang and Strahler 2000), ranging from those with only two or three parameters (e.g. Verstraete *et al.* 1990, Wanner *et al.* 1995, Martonchik *et al.* 2002) to those with 10 or more parameters (e.g. Li and Strahler 1992, Myneni and Asrar 1993). The BRDF model parameters retrieved by inversion of the BRDF models against multiple view angle observations quantify intrinsic surface properties and hence are suited for applications requiring characterization of the directional anisotropy of the Earth's surface reflectance. Simple models containing two or three parameters are the most appropriate for this research because the information content of the available data precludes the use of models with large numbers of parameters. The repeat cycle of the MISR is 16 days. Vegetated surfaces could change significantly during the repeat cycle. Thus, a single swath of the MISR is the most consistent data source from which to obtain BRDF model parameters by inverting the BRDF models against moderate resolution multiangle reflectance data. Each swath of the MISR provides reflectance in nine directions, assuming no obstructions by clouds or topographic features. Although the reflectance in the nine directions are not enough to invert a complicated BRDF model containing 10 or more parameters, they are sufficient to invert a simple BRDF model that contains two or three parameters. This research used the modified Rahman–Pinty–Verstraete (RPV) model (Martonchik *et al.* 2002) and a linear semi-empirical kernel-driven model (Wanner *et al.* 1995) known as the RossThin-LiSparseReciprocal (RTnLS) model. The RPV model is a pure empirical model with three independent parameters. The RTnLS model characterizes the land surface reflectance as a sum of three kernels representing basic scattering types: isotropic scattering, radiative transfer-type volumetric scattering and geometric-optical surface scattering. The semi-empirical RTnLS model also has independent parameters. Thus, a single swath of the MISR can acquire sufficient multiple view angle observations to invert the two BRDF models. This paper uses a modified version of the Algorithm for Moderate Resolution Imaging

Spectroradiometer (MODIS) Bidirectional Reflectance Anisotropies of the Land Surface (AMBRALS; Lucht *et al.* 2000), version 2.4, to adjust the RTnLS model against the MISR multiangle data sets.

As one of the additional features used by the classification algorithms, topographic parameters are widely used in remote sensing (Strahler *et al.* 1978, Jensen 2005, Wilkinson 2005). For example, a dataset might consist of several multispectral bands and several additional features (e.g. percentage slope and aspect) derived from a digital elevation model (DEM). The entire dataset is acted on by the classification algorithms.

A primary objective of this research was to investigate the utility of topographic parameters and BRDF model parameters for vegetation mapping in desert regions. The Jornada Experimental Range and the Sevilleta National Wildlife Refuge in New Mexico were selected as study areas because they have a long history of research and experimentation, making them unique locations to study the effects of climate change on the interface between desert grassland and desert shrub ecosystems and to test different remote sensing techniques and systems for monitoring and detecting these changes (Havstad *et al.* 2000). Currently, the RTnLS BRDF model parameters are routinely provided by the MODIS BRDF/Albedo data product (Schaaf *et al.* 2002), and the RPV BRDF model parameters are routinely provided by the MISR Aerosol/Surface data product (Diner *et al.* 1998). If BRDF model parameters are able to provide useful information in the same way as topographic parameters, but are not highly correlated to the topographic information, it should be possible to realize an increase in classification accuracy.

To gain knowledge of how classification algorithms contribute to increasing accuracy, two classifiers, the maximum likelihood classification (MLC) and the support vector machine (SVM), were used in this research. The MLC and SVM use different mathematical bases, and they have different requirements on training data. As a standard classification method in remote sensing, the MLC is based on the Gaussian model for the distribution of pixels from each class. Thus, data samples for the training MLC should be representative of the classes in order to derive appropriate training statistics on which to base the classification (Campbell 2003). The SVM (Vapnik 1995) classifier, however, depends on data samples that decide the hyperplane separating two classes, called support vectors. Such data samples may poorly describe the typical spectral responses of the classes, which is the requirement for the MLC. In this regard, when additional data are added to a prior dataset, if both the MLC and the SVM obtain increased accuracy, it is a logical outcome that the additional data do contribute to the increase in accuracy. In this research, nadir multispectral reflectance was considered to be the fundamental dataset. The BRDF model parameters, topographic parameters derived from a DEM and their combinations were added incrementally to this fundamental dataset. MLC and SVM classifications were carried out on every dataset to determine whether the additional data are capable of increasing accuracy and in what way the accuracies are raised.

2. Background

2.1 *MISR*

The MISR provides new and unique opportunities to record the anisotropy of land surface reflectance. This instrument consists of nine pushbroom cameras. One camera is directed towards the nadir (designated An), four cameras point in the

forward direction (designated Af, Bf, Cf and Df) and another four cameras point in the aftward direction (designated Aa, Ba, Ca and Da). Images are acquired with nominal view angles, relative to the surface reference ellipsoid, of 0°, 26.1°, 45.6°, 60.0° and 70.5° for An, Af/Aa, Bf/Ba, Cf/Ca and Df/Da, respectively. Each camera uses four spectral bands, whose shapes are approximately Gaussian and centred at 446, 558, 672 and 866 nm. In Global Science mode, the MISR nadir camera is the only one with all four bands at high resolution (275 m). The other eight cameras produce red band data at 275 m resolution, but the remaining bands are averaged to 1.1 km resolution. From the 705-km descending polar orbit of the EOS-AM spacecraft, the zonal overlap swath width of the MISR imaging data is 360 km, which provides global multiangle coverage of the entire Earth in 9 days at the equator and 2 days at the poles. A separate Space-Oblique Mercator (SOM) projection is established for each of the paths of the 233 repeat orbits of the EOS 16-day cycle. The SOM projection minimizes distortion and resampling effects, as its projection meridian nominally follows the spacecraft ground track and a constant distance scale is preserved along that track. The horizontal datum for each projection is the World Geodetic System 1984 (WGS84) ellipsoid. The MISR georectified product removes the errors of the spacecraft position and provides knowledge and errors due to topography. A more complete description of the MISR can be found in Diner *et al.* (1998).

2.2 *RPV model*

The RPV model (Rahman *et al.* 1993, Martonchik *et al.* 2002) predicts the bidirectional reflectance factor (BRF) of an arbitrary surface as a function of the geometry of illumination and observation. Through its mathematical formulation, the RPV model splits a BRF field into its amplitude component and the associated angular field describing the anisotropic behaviour of the surfaces under investigation when illuminated by the Sun, that is:

$$R(\theta_i, \theta_v, \phi) = r0 \frac{\cos\theta_i^{k-1} \cos\theta_v^{k-1}}{(\cos\theta_i + \cos\theta_v)^{1-k}} \exp[b\, p(\Omega)]\, h(\theta_i, \theta_v, \phi) \tag{1}$$

with three free parameters ($r0$, k, b). θ_i is the zenith angle of the direction of illumination by the Sun, θ_v is the zenith angle of the direction of viewing by the sensor, and ϕ is the relative azimuth angle between the direction of illumination and of viewing. Figure 1 shows the geometry of illumination and observation. The function h is a factor to account for the hot spot:

$$h(\theta_i, \theta_v, \phi) = 1 + \frac{1 - r0}{1 + G(\theta_i, \theta_v, \phi)} \tag{2}$$

$$G(\theta_i, \theta_v, \phi) = \left[\left(\frac{\sin\theta_i}{\cos\theta_i} \right)^2 + \left(\frac{\sin\theta_v}{\cos\theta_v} \right)^2 + 2 \left[\frac{\sin\theta_i}{\cos\theta_i} \frac{\sin\theta_v}{\cos\theta_v} \right] \cos\phi \right]^{1/2} \tag{3}$$

The function p in equation (1) is assumed to depend only on the scattering angle Ω, the angle between the directions of the incident and reflected radiances. It is defined as

$$p(\Omega) = \cos(\Omega) = \cos\theta_i \cos\theta_v - \sin\theta_i \sin\theta_v \cos\phi \tag{4}$$

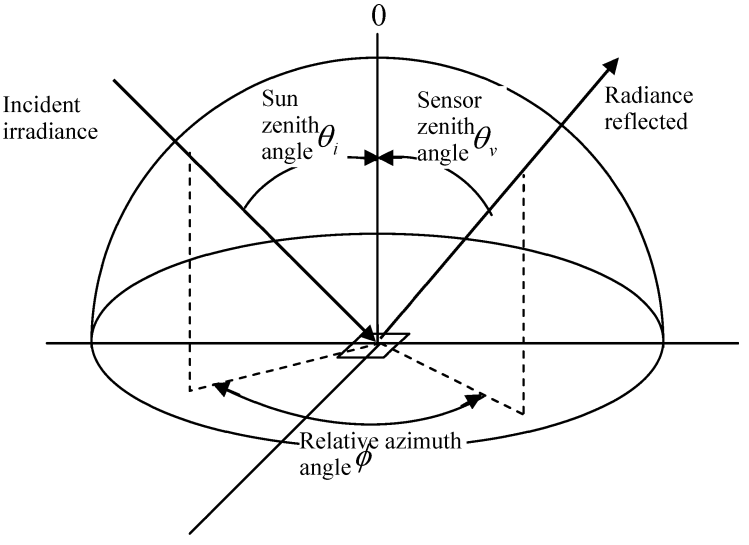

Figure 1. The geometry of illumination and observation.

r0 gives the overall reflectance level, *k* is representative of the bowl or bell shape of the surface anisotropy, and *b* describes the predominance of forward or backward scattering.

2.3 *The semi-empirical kernel-based BRDF model*

A kernel-driven semi-empirical BRDF model was first derived from a physically based BRDF model by Roujean *et al.* (1992) and then developed further by Wanner *et al.* (1995). The semi-empirical models have a simple linear form (equation (5)):

$$BRDF = f_{\text{iso}} + f_{\text{vol}}\, k_{\text{vol}}(\theta_{\text{i}}, \theta_{\text{v}}, \phi) + f_{\text{geo}}\, k_{\text{geo}}(\theta_{\text{i}}, \theta_{\text{v}}, \phi) \tag{5}$$

$$k_{\text{vol}}(\theta_{\text{i}}, \theta_{\text{v}}, \phi) = \frac{(\pi/2 - \xi)\cos\xi + \sin\xi}{\cos\theta_{\text{i}} + \cos\theta_{\text{v}}} - \frac{\pi}{4} \tag{6}$$

$$k_{\text{geo}}(\theta_{\text{i}}, \theta_{\text{v}}, \phi) = O(\theta_{\text{i}}, \theta_{\text{v}}, \phi) - \sec\theta_{\text{i}} - \sec\theta_{\text{v}} + 0.5\,(1 + \cos\xi)\sec\theta_{\text{i}}\sec\theta_{\text{v}} \tag{7}$$

$$O(\theta_{\text{i}}, \theta_{\text{v}}, \phi) = \frac{1}{\pi}(t - \sin t\cos t)(\sec\theta_{\text{i}} + \sec\theta_{\text{v}}) \tag{8}$$

$$\cos t = 2\,\frac{\sqrt{D^2 + (\tan\theta_{\text{i}}\tan\theta_{\text{v}}\sin\phi)^2}}{\sec\theta_{\text{i}} + \sec\theta_{\text{v}}} \tag{9}$$

$$D = \sqrt{\tan^2\theta_{\text{i}} + \tan^2\theta_{\text{v}} - 2\tan\theta_{\text{i}}\tan\theta_{\text{v}}\cos\phi} \tag{10}$$

$$\cos\xi = \cos\theta_{\text{i}}\cos\theta_{\text{v}} + \sin\theta_{\text{i}}\sin\theta_{\text{v}}\cos\phi \tag{11}$$

where k_{vol}, called the RossThick volumetric kernel, is a function of view zenith θ_{v}, illumination zenith θ_{i} and relative azimuth ϕ. k_{vol}, derived from a single-scattering

approximation of radiative transfer theory by Ross (1981), describes the volume scattering from the pixel. k_{geo}, called the LiSparse-Reciprocity geometric kernel, is also a function of θ_v, θ_i and ϕ. k_{geo}, derived from the geometric optical mutual shadowing BRDF model by Li and Strahler (1992), describes the surface scattering from the pixel. f_{vol} and f_{geo} are the weights for these two kernels, respectively. f_{iso} represents the isotropic reflectance.

2.4 *SVM*

An SVM classifier was used in this research to perform the classification experiments because of its excellent empirical performance (Burges 1998). The foundations of the SVM approach were developed by Vapnik (1995). The SVM aims to obtain an optimal separating hyperplane for a training data set in terms of generalization error. Given a set of examples (x_i, y_i), $i=1, \ldots, l$, where $x_i \in R^N$ and $y_i \in \{-1, +1\}$, indicating the class to which the point x_i belongs, when these points are linear separable, the objective of the optimization is to give the maximal-margin hyperplane, which divides the points having $y_i=1$ from those having $y_i=-1$. The hyperplane can be written as:

$$wx=b \tag{12}$$

The vector w is a normal vector; it is perpendicular to the hyperplane. The parameter b determines the offset of the hyperplane from the origin along the normal vector w. The optimization problem can be written as:

$$\min_{w,\,b}|w|, \text{ subject to } y_i(w\,x_i-b)\geq 1, \quad 1\leq i\leq l \tag{13}$$

For non-linear and non-separable cases, the optimization problem was modified as:

$$\min_{w,\,b,\,\xi}\left(\frac{1}{2}w^{\mathrm{T}}\,w+C\sum_{i=1}^{l}\xi_i\right), \text{ subject to } y_i\left(w^{\mathrm{T}}\,\phi(x_i)-b\right)\geq 1-\xi_i,\ \xi_i\geq 0,\ 1\leq i\leq l \tag{14}$$

Here ξ_i are positive slack variables that measure the degree of misclassification of the datum x_i. $C>0$ is a preset penalty value for misclassification errors. Training vector x_i is mapped into a higher (maybe infinite) dimensional space by the function ϕ. $k(x_i, x_j)=\phi(x_i)^T\,\phi(x_j)$ is the kernel function. The choice of the kernel function k is crucial for good classification performance. This research uses the radial basis function (RBF), the most commonly used kernel function:

$$k\left(x_i,\,x_j\right)=\exp\left(-\gamma\left\|x_i-x_j\right\|^2\right),\ \gamma>0 \tag{15}$$

where γ is a kernel parameter. In general, the RBF is a reasonable choice (Chang and Lin 2001). The RBF kernel non-linearly maps samples into a higher dimensional space; thus, although the classifier is a hyperplane in the high-dimensional feature space it may be non-linear in the original input space (Boser *et al.* 1992). The LIBSVM software (Chang and Lin 2001) was used in this research.

To apply the SVM, the following three procedures were used in the experiments (Chang and Lin 2001): first, scaling was conducted on the data. Sarle (1997) explains why the data are usually scaled before their use to train neural networks; most of those considerations are also applied to using a SVM. Second, the best parameters C and γ were searched by fivefold cross-validation on the training set. The goal is to

identify the best (C, γ) so that the classifier can accurately predict unknown data. Third, the best parameters C and γ were used to test the accuracy and calculate the kappa index on the test set.

3. *Study area*

The two study sites in this research are: (1) the Jornada Experimental Range (the Jornada) in southern New Mexico near Las Cruces, and (2) the Sevilleta National Wildlife Refuge (NWR) (the Sevilleta) in central New Mexico near Albuquerque. The Jornada is 78 266 ha and is located in the Jornada del Muerto plain of southern New Mexico (figure 2) between the Rio Grande floodplain on the west and the crest of the San Andres Mountains on the east. Its elevation is from 1176 to 2734 m. The mean annual temperature is approximately 15°C and mean annual rainfall is approximately 210 mm (Havstad *et al.* 2000). More than 50% of the precipitation occurs from July to September. Rain usually comes during the summer monsoon season, which typically begins in early July and can last through August to September. Large stretches of black grama (*Bouteloua eriopoda*) grassland have succeeded in communities dominated by shrubs, most prominently creosote (*Larrea tridentata*) and mesquite (*Prosopis glandulosa*), in the past 100 years (Gibbens *et al.* 2005). The current landscape is a mosaic of grasslands and expanses of relatively bare ground dotted with 'shrub islands'. The second site, the Sevilleta, is one of the largest reserves in the southwest United States and is approximately 100 000 ha in size. It is recognized as having increasing importance in the maintenance of arid-land biodiversity in the region. Its elevation ranges from 1404 to 2719 m. The Sevilleta NWR lies at the junction of four major biomes (Chihuahuan Desert, Great Basin, Rocky Mountains and the Great Plains), abuts two mountain ranges and is traversed by the largest river in New Mexico. The Sevilleta NWR has a wide range of ecosystem types: Chihuahuan Desert, Great Plains Grassland, Great Basin Shrub-Steppe, Piñon-Juniper Woodland, Bosque Riparian Forests, Wetlands and Montane Coniferous Forest. In 1995, the JORNada EXperiment (JORNEX) campaign

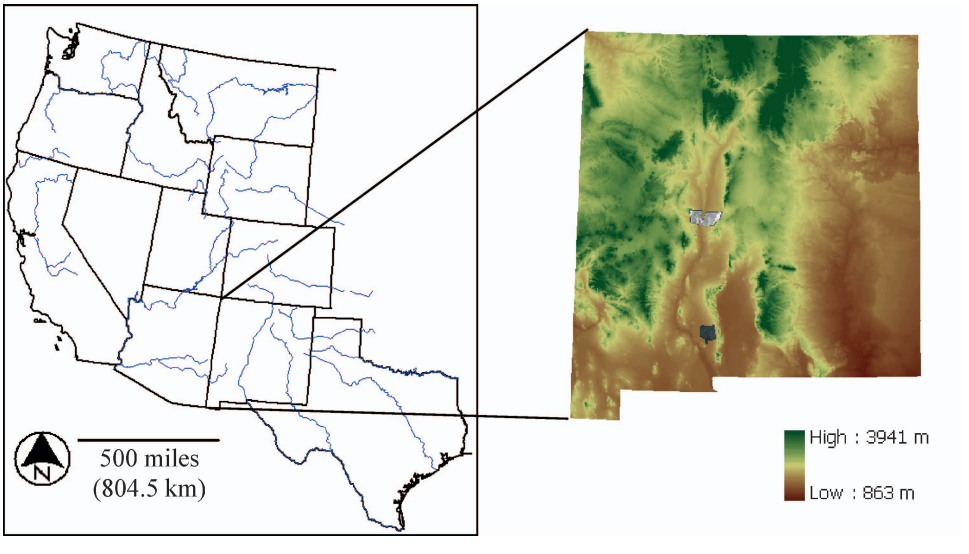

Figure 2. Locations of the Jornada and the Sevilleta.

started to collect remotely sensed data from ground, airborne, and satellite platforms to provide spatial and temporal data on physical and biological states of the Jornada rangeland (Rango *et al.* 1998, Havstad *et al.* 2000).

The vegetation maps produced by the Jornada Long-Term Ecological Research (LTER) and the Sevilleta LTER programmes (Muldavin *et al.* 1998) are used as reference data (figure 3). For the Jornada vegetation map, vegetation types are envisioned as areas greater than 4 ha, where one to four species of plants are dominant. When shrub canopy cover exceeded 5%, they were considered to be the primary dominant vegetation. The Jornada vegetation map has nine classes, each of which has a unique species composition and dominant species. These classes describe the major plant communities. The Sevilleta vegetation map is nominal 0.5 ha spatial resolution, and 13 map classes are derived based on similar vegetation composition and spatial relationships. This research adopts 19 classes from both extensive sites, where six classes are from the Jornada and 13 classes from the Sevilleta (table 1). Although the Jornada vegetation map has nine classes, six classes were adopted. The Bare, Snakeweed and Yucca were excluded, because the numbers of pixels for the three classes were too low to construct valid signatures; they do not provide adequate training data. The Jornada vegetation map uses a set of class names that differ from those used for the Sevilleta vegetation map; this might lead to a misunderstanding that the two study areas have completely different vegetation classes. In fact, both sites are within the Chihuahuan Desert. A number of the shrub and grass communities are similar (e.g. black grama, galleta grass, creosotebush, mesquite), although they use different vegetation classes in different classification systems. It is reasonable to classify the two study areas together. The total

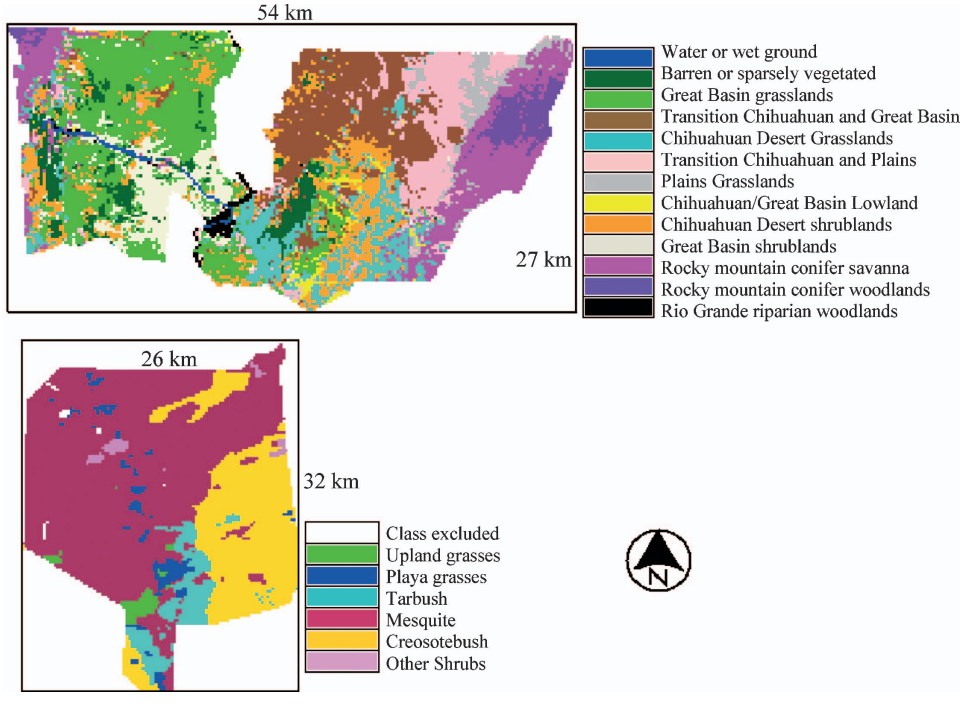

Figure 3. Vegetation maps of the Jornada and the Sevilleta.

Table 1. The six classes of the Jornada and the 13 classes of the Sevilleta.

Jornada Experimental Range	
1	Upland black grama grassland
2	Playa dropseed grassland
3	Tarbush shrubland
4	Mesquite shrubland
5	Creosotebush shrubland
6	Mixed shrubland
Sevilleta National Wildlife Refuge	
7	Water or wet ground
8	Barren or sparsely vegetated land
9	Galleta/India ricegrass (Great Basin grasslands)
10	Black grama/Galleta transition grasslands (Transition Chihuahuan and Great Basin grasslands)
11	Black grama grassland (Chihuahuan Desert grasslands)
12	Black/Blue grama grassland (Transition Chihuahuan and Plains grasslands)
13	Blue/Hairy grama grassland (Plains grasslands)
14	Chihuahuan or Great Basin lowlandswale grasslands
15	Creosotebush shrubland (Chihuahuan Desert shrublands)
16	Fourwing saltbush/Broom daleta shrubland (Great Basin shrublands)
17	Conifer_Savanna (Rocky Mountain conifer savanna)
18	Conifer_Woodlands (Rocky Mountain conifer woodlands)
19	Riparian_Woodlands (Rio Grande river riparian woodlands)

experimental area covered by the Jornada and Sevilleta vegetation maps is 23 978 pixels (250 m spatial resolution), covering approximately 1498 km^2.

4. Method

This research used MISR orbit O013039 data from 31 May 2002. This study used three MISR data products: (1) the MISR level 1B2 MI1B2T terrain-projected product, (2) the MISR level 1B2 MI1B2GEOP geometric parameters product, and (3) the MISR level 2 MIL2ASAE aerosol product. The first product, the MI1B2T product, is the terrain-projected top-of-atmosphere (TOA) radiance with 1.1 km resolution (the off-nadir viewing and non-red bands) and 275 m resolution (the nadir viewing or red band). The second product, the MI1B2GEOP product, provides solar zenith, solar azimuth and nine viewing zenith and azimuth angles at 17.6 km resolution. The third product, the MIL2ASAE product, delivers aerosol optical depth (AOD) with 17.6 km resolution. A kriging method was used to smooth the MIL2ASAE 17.6 km AOD data prior to atmospheric correction. MI1B2T TOA radiance was corrected for atmospheric absorption and scattering using the Simplified Method for Atmospheric Correction (SMAC) algorithm (Rahman and Dedieu 1994), which uses the desert coefficients of the MISR sensor atmospheric correction. The solar zenith, solar azimuth, viewing zenith and azimuth angles were from the MI1B2GEOP product. The aerosol concentration used was the regional mean spectral optical depth from the MIL2ASAE product. The surface reflectance was then resampled to the Universal Transverse Mercator (UTM) map projection, WGS84 spheroid/datum, zone 13N, with a grid interval of 250 m. As a consequence, the MISR multiple angle dataset was produced, including four nadir multispectral reflectances and eight off-nadir red and near-infrared (NIR) bidirectional reflectances.

To study the utility of BRDF model parameters and topographic parameters for mapping vegetation in the study area, the following two steps were carried out to produce the experiment dataset:

(1) The BRDF parameters (the *r0*, *k*, *b*, f_{iso}, f_{vol} and f_{geo} at red and NIR bands) were derived by inverting the RPV and RTnLS models against the nine (one nadir plus eight off-nadir) directional reflectance estimates in the red and NIR bands.

(2) To derive the topographic parameters, the original DEM data (spatial resolution 10 m of the Jornada data (http://usda-ars.nmsu.edu/data.html) and 30 m of the Sevilleta data (http://sevilleta.unm.edu/data/archive/gis/)) were scaled up to 250 m spatial resolution by computing the mean and deviation to match the resolution of the MISR data. In total, six data layers were generated: (1) the mean of elevation, (2) the standard deviation of elevation, (3) the mean of the slope, (4) the standard deviation of the slope, (5) the mean of the aspect, and (6) the standard deviation of the aspect. The standard deviation is a measure that indicates how tightly all the various examples are clustered around the mean. At the beginning, it was expected that it would be best for the classification to use the means and standard deviations together. However, using the standard deviations and the means along with the MISR data (the nadir spectral reflectance and the BRDF parameters) did not provide greater classification accuracy than when using only the means with the MISR data. Therefore, only the three means (elevation, slope and aspect) were used as additional data for the semi-arid vegetation mapping in this research.

In total, 32 experiments were carried out to evaluate the accuracy increase produced by the BRDF model parameters and the topographic parameters. The 32 experiments were based on 16 datasets with MLC and the SVM. These 16 datasets (listed in tables 2 and 3) are combinations of the following basic datasets: (1) one dataset of the MISR 4 nadir spectral reflectance (blue, green, red and NIR), called MISR-nadir; (2) one dataset of the BRDF model parameters (*r0*, *k*, *b* and f_{iso}, f_{vol} and f_{geo} at red and NIR bands), called BRDF parameters, and (3) eight datasets of topographic parameters (i.e. (1) including no topographic parameters, (2) elevation, (3) slope, (4) aspect, (5) elevation and slope, (6) elevation and aspect, (7) slope and aspect, and (8) elevation, slope and aspect), called topographic parameters. The

Table 2. Classifications and their accuracies with the MLC.

Topographic parameters	MISR-nadir		MISR-nadir + BRDF parameters		
	Overall1/kappa	*Change0*	*Overall2*/kappa	*Change1*	*Change2*
None	45.8/41.1	NA	65.9/62.1	NA	NA
Elevation	53.8/49.7	+8.0	66.7/62.9	+0.8	+12.9
Slope	51.7/47.0	+6.0	66.5/62.6	+0.6	+14.8
Aspect	49.3/44.7	+3.8	66.3/62.5	+0.4	+17.0
Elevation, Slope	56.5/52.3	+10.7	67.5/63.8	+1.6	+11.0
Slope, Aspect	53.8/49.2	+8.0	67.1/63.3	+1.2	+13.3
Elevation, Aspect	56.0/51.9	+10.2	67.4/63.7	+1.3	+11.4
Elevation, Aspect, Slope	57.7/53.5	+11.9	67.7/64.0	+1.8	+10.0

Table 3. Classifications and their accuracies with the SVM.

Topographic parameters	MISR-nadir		MISR-nadir + BRDF parameters		
	Overall1/kappa	*Change0*	*Overall2*/kappa	*Change1*	*Change2*
None	64.3/59.1	N/A	75.6/72.2	N/A	N/A
Elevation	72.7/68.8	+8.4	76.6/73.4	+1.0	+3.9
Slope	67.1/62.3	+2.8	75.6/72.3	0.0	+8.5
Aspect	65.7/60.3	+1.0	75.3/72.0	−0.3	+9.5
Elevation, Slope	72.9/69.1	+8.6	76.6/73.4	+1.0	+3.7
Slope, Aspect	67.7/63.0	+3.4	75.7/72.3	+0.1	+8.0
Elevation, Aspect	72.3/68.4	+8.0	76.4/73.1	+0.8	+4.1
Elevation, Aspect, Slope	72.5/68.6	+8.2	76.0/72.8	+0.4	+3.5

MISR-nadir was considered as the baseline because nadir observation is the basic remote sensing observation. The BRDF and the topographic parameters were considered as additional information to increase the classification accuracy from the baseline (the MISR-nadir).

The accuracy of the MISR-nadir was the benchmark for all of the other experiments. To assess the impact of the BRDF parameters and the topographic parameters on the classification accuracy, the following tasks were implemented in a sequence:

(1) The accuracy of the MISR-nadir plus the BRDF parameters was investigated. The purpose was to examine the accuracy increase by incorporating the BRDF parameters into the nadir observations.
(2) The accuracy of the MISR-nadir plus the topographic parameters was investigated. The purpose was to explore the capability of the topographic parameters in the accuracy increase. In addition, by comparing the results of the MISR-nadir plus the BRDF parameters with the MISR-nadir plus the topographic parameters, we aimed to determine whether the BRDF or the topographic parameters were more suitable to increase accuracy.
(3) The accuracy of the MISR-nadir plus both the BRDF parameters and topographic parameters were investigated together. The purpose was to examine whether the BRDF parameters and the topographic parameters in combination could help to increase the accuracy. If the accuracy increase was significant after combining both the BRDF parameters and the topographic parameters together with the MISR-nadir, it would encourage the use of the two kinds of information together for this semi-arid vegetation mapping.

5. Results and discussion

Tables 2 and 3 present the results of the 32 experiments, including the 16 classifications with the MLC and the SVM. The classification accuracies for the MLC and SVM classifiers are shown in figures 4 and 5, respectively. In addition to the overall accuracy and kappa coefficient, three kinds of accuracy changes in each experiment are also displayed: (1) the difference between accuracies of the MISR-nadir plus the topographic parameters and those of the MISR-nadir, indicated by *change0*; (2) the difference between accuracies of the MISR-nadir plus the

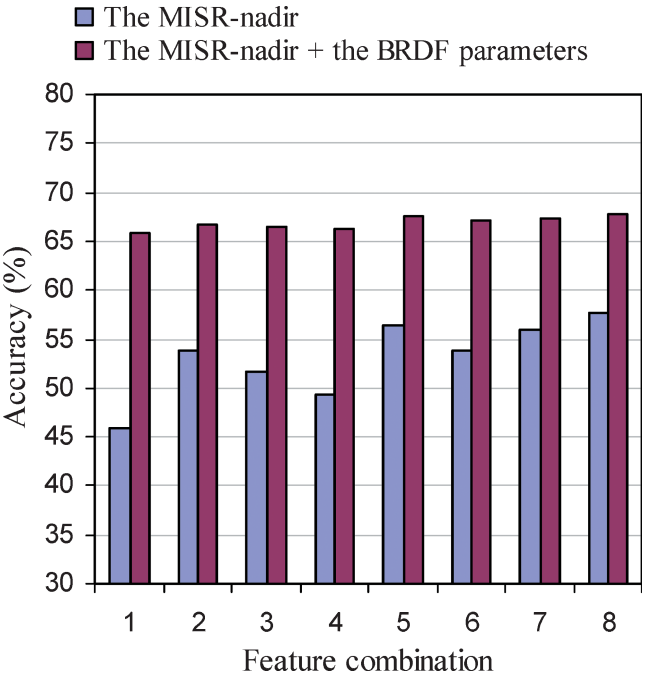

Figure 4. Accuracy of 16 combinations of (the MISR-nadir or the MISR-nadir + the BRDF parameters) and topographic parameters: 1, no topographic parameters; 2, elevation; 3, slope; 4, aspect; 5, elevation and slope; 6, slope and aspect; 7, elevation and aspect; 8, elevation and aspect and slope. The MLC was used here.

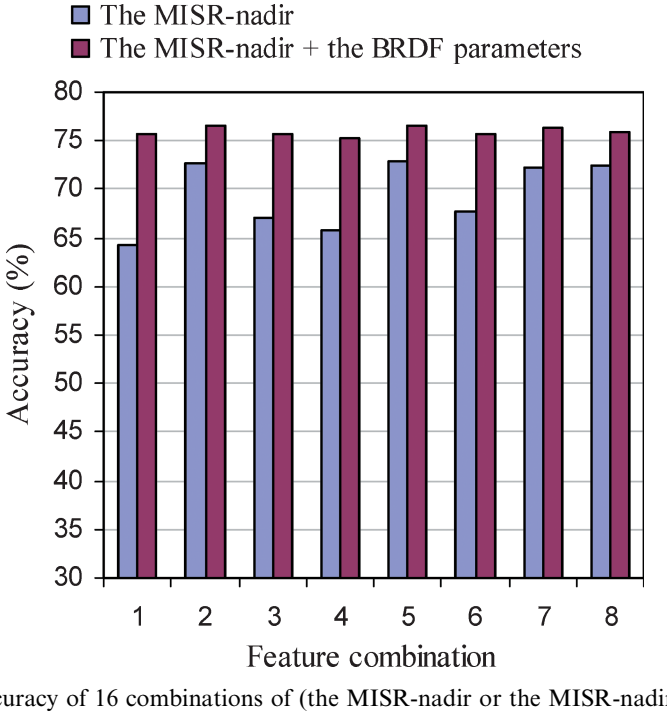

Figure 5. Accuracy of 16 combinations of (the MISR-nadir or the MISR-nadir + the BRDF parameters) and topographic parameters: 1, no topographic parameters; 2, elevation; 3, slope; 4, aspect; 5, elevation and slope; 6, slope and aspect; 7, elevation and aspect; 8, elevation and aspect and slope. The SVM was used here.

topographic parameters and BRDF parameters together and that of the MISR-nadir plus BRDF parameters, indicated by *change1*; and (3) the difference between accuracies obtained on the MISR-nadir plus the topographic parameters and the BRDF parameters together and accuracies obtained on the MISR-nadir plus topographic parameters, indicated by *change2*. The purpose of the accuracy changes was to clearly show the capability of the topographic parameters and of the BRDF parameters to improve the recognition of semi-arid vegetation types. The kappa coefficient can be thought of as the chance-corrected proportional agreement, and possible values range from +1 (perfect agreement) to 0 (no agreement above that expected by chance) to −1 (complete disagreement). More specifically, a kappa coefficient can be interpreted as follows: <0.40 is low agreement, 0.41–0.60 is moderate agreement, and 0.61–0.80 is full agreement.

Tables 2 and 3 show that both the BRDF parameters and the topographic parameters can increase the classification accuracy, regardless of whether the MLC or the SVM is applied. In other words, the results suggest that the reasons for the increased accuracy are mainly due to adding new data. For instance, adding the BRDF parameters on the MISR-nadir brings approximately 20% and 11% increments on the MLC and SVM classifiers, respectively. The increased accuracy from adding the topographic parameters on the MISR-nadir is around 12% using the MLC when elevation, slope and aspect are used together; and 9% using the SVM when elevation and slope are used together. This illustrates that both the BRDF parameters and the topographic parameters can provide useful information for this semi-arid vegetation mapping. Furthermore, when adding the BRDF parameters and the topographic parameters on the MISR-nadir, the highest accuracy is 67.7% with the MLC and 76.6% with the SVM. These are more than 21% and 12% increments compared with only the MISR-nadir used with the MLC and SVM, respectively. The difference between the two highest accuracies is almost 10%. This illustrates that the topographic parameters and the BRDF parameters can raise the accuracy higher for the MLC than for the SVM. However, we should point out that the accuracy of the MISR-nadir is 64.3% for the SVM and 45.8% for the MLC, a difference of almost 20%, indicating that the SVM can obtain knowledge from the data more efficiently than the MLC.

Of note, according to *change1* in tables 2 and 3, the topographic parameters can only add less than 2% and 1% accuracy for a dataset of the MISR-nadir plus the BRDF parameters with the MLC and SVM, respectively. According to *change2* in tables 2 and 3, the BRDF parameters can add more than 10% and 3.5% accuracy for a dataset of the MISR-nadir plus the topographic parameters with the MLC and SVM, respectively. In other words, the accuracy increment by adding the BRDF parameters on a dataset of the MISR-nadir and topographic parameters together is much greater than by adding the topographic parameters on a dataset of the MISR-nadir and the BRDF parameters together. This suggests that the BRDF parameters can provide more additional information to the nadir multispectral data than the topographic parameters for this semi-arid vegetation mapping. The reasons may be twofold. First, the BRDF parameters carry structural information about vegetation, and structural information on the canopy is usually directly related to vegetation type. Second, vegetation community types may not have a strong correlation with topographic parameters in the Jornada and the Sevilleta areas. In addition, scale issues of the topographic information may also affect contribution to vegetation type mapping. Instead of elevation, slope and aspect, we may need some new parameters to characterize the complexity of the topography in a remote sensing pixel.

To compare the improvement obtained by adding the topographic parameters to those obtained by adding the BRDF parameters, tables 4 and 5 give the producer's accuracy, the user's accuracy and increases in the user's accuracy for the MLC and SVM for the four most informative cases, respectively. The four experiments are (1) the MISR-nadir, (2) the MISR-nadir plus the topographic parameters (e.g. elevation and slope for SVM; elevation, slope and aspect for MLC), (3) the MISR-nadir plus the BRDF parameters, and (4) the MISR-nadir plus the topographic parameters and BRDF parameters. The user's accuracies for these four experiments are shown in figures 6 and 7.

The MISR-nadir dataset with the MLC method produces serious misclassifications (see 'Nadir accuracy' in table 4). This highlights the limitations of the nadir-spectral data in this environment. The improvements in differentiating these classes when adding the BRDF parameters on the MISR-nadir dataset are perhaps not surprising given that the multiangle data and metrics hold greater information on canopy structure ('BRDF accuracy' in table 4). This information is derived mainly from the change in the proportion of shadowed soil in the multiple angle observations. All classes except class 4 increase accuracy, compared with accuracy of the MISR-nadir ('BRDF Inc_n' in table 4). In particular, 11 out of 18 classes show a 10% or more accuracy increase. This is a considerable increase, especially in the vegetation type mapping at the community level. The apparent improvements in differentiating these classes when adding the topographic parameters on the MISR-nadir are perhaps not unexpected because the vegetation cover is also associated with topography and soil to some degree ('Elevation-slope accuracy' in table 4). Sixteen out of 19 classes have an increase in accuracy and four out of 16 classes have a 10% or more increase in accuracy, compared with that of the MISR-nadir ('Topographic Inc_n' in table 4).

Clearly, the best improvement is obtained when adding both the BRDF parameters and the topographic parameters to the MISR-nadir ('All accuracy' in table 4). Compared with the accuracy of the MISR-nadir ('All Inc_n' in table 4), 18 out of 19 classes have an increase in accuracy and 12 out of 18 classes have an increase of 10% or more. Compared to the accuracy of the MISR-nadir plus the BRDF parameters ('All Inc_a' in table 4), 14 out of 19 classes have an increase in accuracy. Compared with the accuracy of the MISR-nadir plus the topographic parameters ('All Inc_e' in table 4), 16 out of 19 classes have an increase in accuracy, and the greatest improvement occurs in class 6 ('Mixed shrubland'). This is now 40% from 3.2% of the MISR-nadir, 18.0% of the MISR-nadir plus the BRDF parameters and 7.3% of the MISR-nadir plus the topographic parameters. For this mixed shrubland, these results suggest that because they offer additional information, BRDF parameters create a greater increase in accuracy than topographic parameters in this environment. Furthermore, the topographic parameters and BRDF parameters complement each other very well.

With regard to the experiments with the SVM algorithm, the SVM always produces better accuracy than the MLC on every corresponding dataset. The MISR-nadir with SVM ('Nadir accuracy' in table 5) provides much better accuracy than that with MLC ('Nadir accuracy' in table 4). Here, 15 out of 19 classes enjoy a higher accuracy than the MISR-nadir/MLC case. This shows that SVM has a stronger capability of obtaining information from data than the MLC. Classes 5 (Creosotebush), 6 (Mixed shrub), 9 (Galleta/India ricegrass) and 17 (Conifer_Savanna), however, have a decrease in accuracy. This is surprising because

Table 4. User's accuracy and producer's accuracy of the MLC.

	Producer's accuracy				User's accuracy								
					Nadir	BRDF		Topographic		All			
Class	Nadir	BRDF	Topographic	All	Accuracy	Accuracy	Inc_n	Accuracy	Inc_n	Accuracy	Inc_n	Inc_a	Inc_e
1	76.1	83.1	93.0	83.1	17.1	34.5	17.4	21.2	4.1	33.7	16.6	−0.8	12.5
2	45.3	64.2	56.1	61.5	16.5	22.8	6.3	19.0	2.5	21.7	5.2	−1.1	2.7
3	64.6	80.3	73.8	84.7	35.6	43.1	7.5	40.6	5.0	43.8	8.2	0.7	3.2
4	47.6	77.5	61.2	78.4	94.1	91.3	−2.8	95.1	1.0	92.0	−2.1	0.7	−3.1
5	34.2	60.1	71.1	68.3	64.1	85.8	21.7	80.6	16.5	89.3	25.2	3.5	8.7
6	79.6	61.2	69.4	53.1	3.2	18.0	14.8	7.3	4.1	40.0	36.8	22.0	32.7
7	50.9	66.0	58.5	66.0	13.3	40.7	27.4	20.7	7.4	42.7	29.4	2.0	22.0
8	52.9	57.8	57.6	60.0	38.6	56.0	17.4	39.1	0.5	55.3	16.7	−0.7	16.2
9	59.4	66.5	48.9	65.7	58.9	72.2	13.3	64.7	5.8	73.6	14.7	1.4	8.9
10	48.5	70.1	57.3	71.0	52.3	71.6	19.3	63.1	10.8	71.6	19.3	0.0	8.5
11	11.2	54.1	24.9	56.4	36.9	45.3	8.4	35.6	−1.3	47.7	10.8	2.4	12.1
12	41.1	56.4	55.0	54.7	44.2	70.2	26.0	53.7	9.5	72.3	28.1	2.1	18.6
13	71.5	66.7	59.7	64.0	30.2	48.3	18.1	36.6	6.4	49.2	19.0	0.9	12.6
14	43.6	65.3	55.7	71.0	12.4	19.6	7.2	11.9	−0.5	20.3	7.9	0.7	8.4
15	12.4	28.6	30.0	32.2	30.2	48.6	18.4	53.1	22.9	53.0	22.8	4.4	−0.1
16	32.9	66.3	51.3	68.5	21.1	52.4	31.3	36.5	15.4	52.9	31.8	0.5	16.4
17	58.4	70.1	64.6	71.0	76.7	77.8	1.1	83.4	6.7	79.5	2.8	1.7	−3.9
18	91.9	89.9	91.9	89.9	67.5	76.6	9.1	68.3	0.8	73.8	6.3	−2.8	5.5
19	62.5	68.1	69.4	73.6	48.9	51.6	2.7	47.2	−1.7	49.5	0.6	−2.1	2.3

Table 5. User's accuracy and producer's accuracy of the SVM.

	Producer's accuracy				User's accuracy								
					Nadir	BRDF		Topographic		All			
Class	Nadir	BRDF	Topographic	All	Accuracy	Accuracy	Inc_n	Accuracy	Inc_n	Accuracy	Inc_n	Inc_a	Inc_e
1	35.2	62.0	52.1	63.4	41.0	69.8	28.8	57.8	16.8	77.6	36.6	7.8	19.8
2	30.4	37.8	34.5	36.5	70.3	74.7	4.4	64.6	−5.7	70.1	−0.2	−4.6	5.5
3	46.6	72.8	62.9	72.1	59.3	67.9	8.6	67.5	8.2	71.1	11.8	3.2	3.6
4	92.6	95.7	94.6	95.6	86.4	90.1	3.7	89.9	3.5	91.3	4.9	1.2	1.4
5	64.5	82.2	86.1	87.5	60.3	89.2	28.9	88.3	28.0	90.1	29.8	0.9	1.8
6	0.0	18.4	20.4	24.5	0.0	50.0	50.0	52.6	52.6	80.0	80.0	30.0	27.4
7	11.3	47.2	28.3	52.8	33.3	59.5	26.2	46.9	13.6	54.9	21.6	−4.6	8.0
8	38.5	53.9	47.8	54.2	65.6	69.1	3.5	68.5	2.9	69.4	3.8	0.3	0.9
9	80.9	84.1	81.8	84.7	54.5	69.0	14.5	61.7	7.2	69.0	14.5	0.0	7.3
10	68.7	79.1	73.7	77.3	56.1	74.4	18.3	67.6	11.5	77.5	21.4	3.1	9.9
11	28.1	52.1	41.3	54.4	40.4	54.7	14.3	48.1	7.7	55.8	15.4	1.1	7.7
12	52.2	67.9	62.4	65.0	57.2	72.4	15.2	70.3	13.1	71.0	13.8	−1.4	0.7
13	52.2	57.5	58.8	60.1	58.3	68.2	9.9	60.6	2.3	62.6	4.3	−5.6	2.0
14	12.1	38.7	19.4	27.4	35.7	40.7	5.0	34.8	−0.9	44.7	9.0	4.0	9.9
15	23.1	40.6	40.0	44.4	36.5	49.7	13.2	52.2	15.7	55.2	18.7	5.5	3.0
16	19.4	57.7	46.5	64.5	38.3	70.4	32.1	56.5	18.2	61.6	23.3	−8.8	5.1
17	74.7	81.0	80.6	80.4	74.0	77.3	3.3	77.8	3.8	78.9	4.9	1.6	1.1
18	78.2	80.2	80.2	79.4	80.5	81.6	1.1	84.0	3.5	83.5	3.0	1.9	−0.5
19	38.9	61.1	69.4	62.5	66.7	74.6	7.9	74.6	7.9	77.6	10.9	3.0	3.0

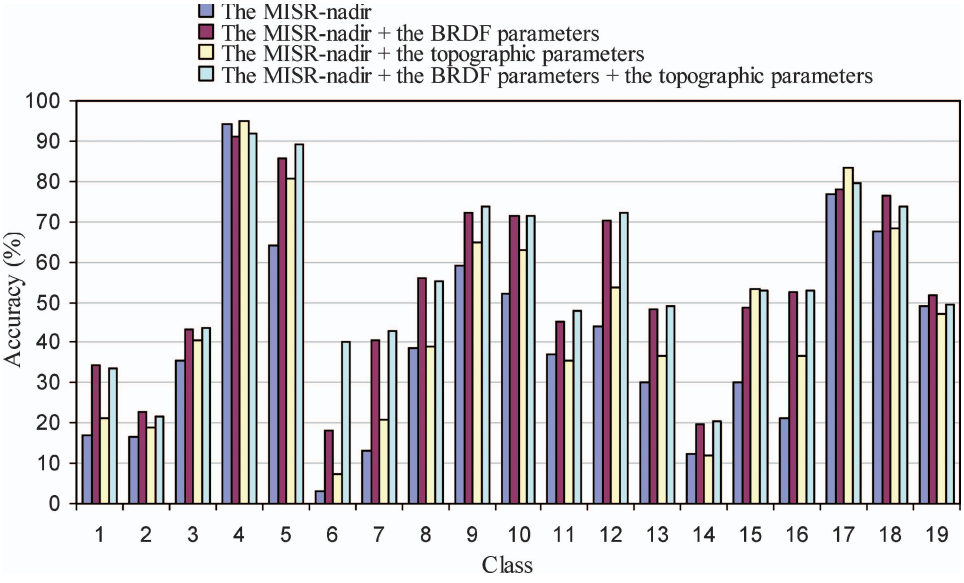

Figure 6. User's accuracy of the four experiments when the MLC was used. The topographic parameters consist of elevation, slope and aspect.

the accuracy reduction classes include all of the main vegetation structures: grass, shrub and tree. This highlights one of the major challenges in classification of remote sensing data; all elements in the sensor's instantaneous field of view contribute to the signal ('pixels are always mixed') and the effects of shadowing are not straightforward to incorporate.

Comparing the results of the MISR-nadir ('Nadir accuracy' in table 5) and the results of the MISR-nadir plus the BRDF parameters ('BRDF accuracy' in table 5), it can be

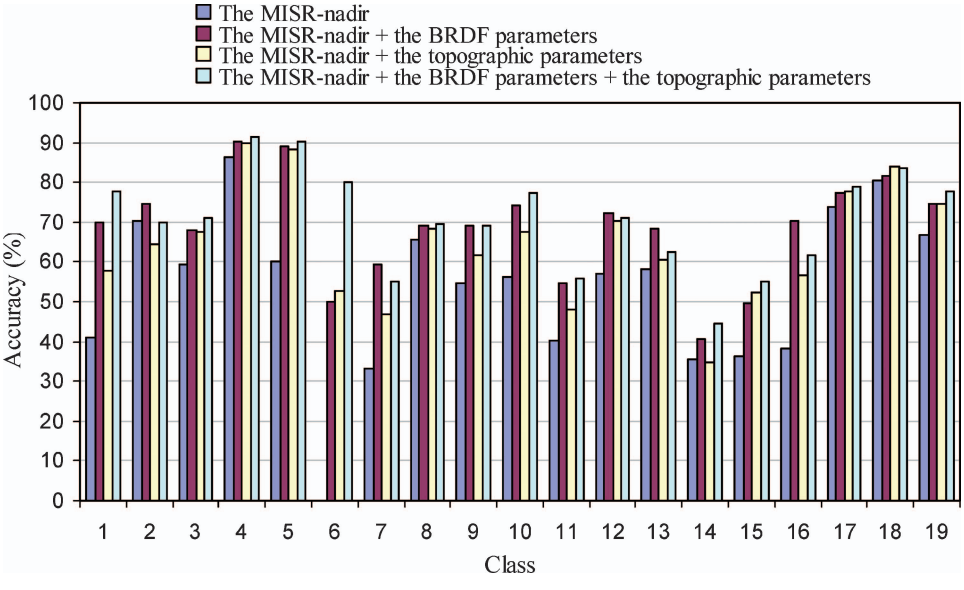

Figure 7. User's accuracy of the four experiments when the SVM was used. The topographic parameters consist of elevation and slope.

seen that all classes have accuracy increases. In 11 out of 19 classes the accuracy increases are very close to or more than 10% ('Anisotropic Inc_n' in table 5). Although the user's accuracy of class 14 (the Sevilleta Chihuahuan or Great Basin Lowland Swale Grasslands) is still low at 40.7% in the MISR-nadir plus the BRDF parameters, this represents an increase of 5% from 35.7% of the MISR-nadir. These statistics indicate that the BRDF parameters improve the classification accuracy.

With the SVM algorithm, adding topographic parameters on the MISR-nadir dataset ('Topographic accuracy' in table 5) leads to an increase in accuracy in 17 out of 19 classes. Importantly, the accuracy increases of eight classes are very close to or more than 10% ('Topographic Inc_n' in table 5). Only two classes have lower accuracy than those of the MISR-nadir dataset. The differences in these two classes are that class 2 (Jornada Playa Grasses) is 5.7% from 70.3% to 64.6%, and class 14 (Chihuahuan or Great Basin lowlandswale grasslands) is 0.7% from 35.7% to 34.8%. The accuracy increases are clearly considerable, and the accuracy decreases are small.

Regarding the SVM algorithm, the best results are achieved when incorporating both the topographic parameters and the BRDF parameters into the MISR-nadir ('All accuracy' in table 5). Compared to the accuracy of the MISR-nadir dataset ('All Inc_n' in table 5), 18 out of 19 classes have an increase in accuracy and 12 out of 18 classes increase 10%. Compared with the accuracy of the MISR-nadir plus the BRDF parameters ('All Inc_a' in table 5), 13 out of 19 classes have a higher accuracy than the MISR plus the BRDF parameters enjoy an accuracy increase. Specifically, the greatest increase is over 30% (class 6, 'Mixed shrubland', from 50.0% to 80.0%); the next is close to 8% (class 1 'Upland black grama grassland' from 77.6% to 69.8%). All the other increases, however, are under 6%. At the same time, the greatest decrease is also more than 5%: class 16 ('Great Basin shrublands') decreases 8.8% from 70.4% to 61.6%, and class 13 ('Plains grasslands') falls 5.5% from 68.2% to 62.6%. Compared to the accuracy of the MISR-nadir plus the topographic parameters, all classes except class 18 have an increase in accuracy ('All Inc_e' in table 5); however, only two out of 18 classes increase 10%. These experiments suggest that both the topographic parameters and the BRDF parameters can provide additional useful information for this semi-arid vegetation mapping. Moreover, the BRDF parameters are slightly more efficient than the topographic parameters. A possible reason is that there may not be a strong association between vegetation types and topography in the desert regions. However, the BRDF parameters provide information about the directional anisotropy of the surface reflectance for classification. This information is mainly determined by heterogeneous three-dimensional structure of vegetation. Therefore, it is not surprising that the BRDF parameters have better performances. The proposed method should be useful in vegetation mapping areas where vegetation types have different canopy physiognomies.

Evidently, using the BRDF parameters provides a clear advantage when classifying areas that do not have adequate DEM data because these BRDF parameters are provided by MODIS and MISR data products routinely, which cover the Earth daily or weekly.

6. Conclusion

In the context of mapping semi-arid vegetation types at moderate resolution, the findings in this research are: (1) both the topographic parameters and the BRDF parameters can provide additional useful information for semi-arid vegetation mapping at the Jornada Experimental Range and the Sevilleta National Wildlife Refuge. (2) In the semi-arid environment, the BRDF parameters are slightly more

efficient than the topographic parameters. BRDF model parameters derived from MODIS and MISR data products have considerable utility in increasing the accuracy of moderate resolution vegetation mapping, by allowing exploitation of the additional information they provide.

Acknowledgements

This research was supported by NASA (EOS grant no. NNG04GK91G to M.J.C., administered through the NASA Land Cover Land Use Change program). The Jornada data sets were provided by the Jornada Basin LTER project. Funding for these data was provided by the U.S. National Science Foundation (Grant DEB-0080412). The MISR data were obtained from the NASA Langley Atmospheric Sciences Data Center.

References

ABUELGASIM, A.A., GOPAL, S., IRONS, J.R. and STRAHLER, A.H., 1996, Classification of ASAS multiangle and multispectral measurements using artificial neural networks. *Remote Sensing of Environment*, **57**, pp. 79–87.

AKBARI, M., MAMANPOUSH, A.R., GIESKE, A., MIRANZADEH, M., TORABI, M. and SALEMI, H.R., 2006, Crop and land cover classification in Iran using Landsat 7 imagery. *International Journal of Remote Sensing*, **27**, pp. 4117–4135.

ARMSTON, J.D., SCARTH, P.F., PHINN, S.R. and DANAHER, T.J., 2007, Analysis of multi-date MISR measurements for forest and woodland communities, Queensland, Australia. *Remote Sensing of Environment*, **107**, pp. 287–298.

ASNER, G.P., 2000, Contributions of multi-view angle remote sensing to land-surface and biogeochemical research. *Remote Sensing Review*, **18**, pp. 137–162.

BOSER, B.E., GUYON, I.M. and VAPNIK, V.N., 1992, A training algorithm for optimal margin classifiers. In *5th Annual ACM Workshop on COLT*, D. Haussler (Ed.) pp. 144–152 (Pittsburgh, PA: ACM Press).

BURGES, C.J.C., 1998, A tutorial on support vector machines for pattern recognition. *Data Mining and Knowledge Discovery*, **2**, pp. 121–167.

CAMPBELL, J.B., 2003, *Introduction to Remote Sensing*, 3rd edn (London: Taylor & Francis).

CHANG, C.C. and LIN, C.J., 2001, *LIBSVM: A Library for Support Vector Machines*. Available online at: www.csie.ntu.edu.tw/~cjlin/libsvm (accessed 15 October 2007).

CHEN, J.M. and CIHLAR, J., 1995, Quantifying the effect of canopy architecture on optical measurements of leaf area index using two gap size analysis methods. *IEEE Transactions on Geoscience and Remote Sensing*, **33**, pp. 777–787.

CHOPPING, M.J., RANGO, A. and RITCHIE, J.C., 2002, Improved semi-arid community type differentiation with the NOAA AVHRR via exploitation of the directional signal. *IEEE Transactions on Geoscience and Remote Sensing*, **40**, pp. 1132–1149.

DINER, D., ASNER, G.P., DAVIES, R., KNYAZIKHIN, Y., MULLER, J.P., NOLIN, A., PINTY, B., SCHAAF, C.B. and STROEVE, J., 1999, New directions in Earth observing: scientific applications of multi-angle remote sensing. *Bulletin of the American Meteorological Society*, **80**, pp. 2209–2228.

DINER, D.J., BECKERT, J.C., REILLY, T.H., BRUEGGE, C.J., CONEL, J.E., KAHN, R.A., MARTONCHIK, J.V., ACKERMAN, T.P., DAVIES, R., GERSTL, S.A.W., GORDON, H.R., MULLER, J.-P., MYNENI, R.B., SELLERS, P.J., PINTY, B. and VERSTRAETE, M.M., 1998, Multi-angle Imaging SpectroRadiometer (MISR) instrument description and overview. *IEEE Transactions on Geoscience and Remote Sensing*, **36**, pp. 1072–1087.

DINER, D.J., MARTONCHIK, J.V., KAHN, R.A., PINTY, B., GOBRON, N., NELSON, D.L. and HOLBEN, B.N., 2005, Using angular and spectral shape similarity constraints to improve MISR aerosol and surface retrievals over land. *Remote Sensing of Environment*, **94**, pp. 155–171.

GIBBENS, R.P., MCNEELY, R.P., HAVSTAD, K.M., BECK, R.F. and NOLEN, B., 2005, Vegetation changes in the Jornada basin from 1858 to 1998. *Journal of Arid Environments*, **61**, pp. 651–668.

GOBRON, N., BINTY, B., VERSTRAETE, M.M., MARTONCHIK, J.V., KNYAZIKHIN, Y. and DINER, D.J., 2000, Potential of multiangular spectral measurements to characterize land surfaces: conceptual approach and exploratory application. *Journal of Geophysical Research*, **105**, pp. 17539–17549.

HAVSTAD, K.M., KUSTAS, W.P., RANGO, A., RITCHIE, J.C. and SCHMUGGE, T.J., 2000, Jornada Experimental Range: a unique arid land location for experiments to validate satellite systems and to understand effects of climate change. *Remote Sensing of Environment*, **74**, pp. 13–25.

LANGLEY, S.K., CHESHIRE, H.M. and HUMES, K.S., 2001, A comparison of single date and multitemporal satellite image classifications in a semi-arid grassland. *Journal of Arid Environments*, **49**, pp. 401–411.

LI, X. and STRAHLER, A.H., 1992, Geometric-optical bidirectional reflectance modeling of the discrete crown vegetation canopy: effect of crown shape and mutual shadowing. *IEEE Transactions on Geosciences and Remote Sensing*, **30**, pp. 276–292.

LIANG, S. and STRAHLER, A., 2000, Land surface bi-directional reflectance distribution function (BRDF): recent advances and future prospects. *Remote Sensing Reviews*, **18**, pp. 83–511.

LIESENBERG, V., GALVÃO, L.S. and PONZONI, F.J., 2007, Variations in reflectance with seasonality and viewing geometry: implications for classification of Brazilian savanna physiognomies with MISR/Terra data. *Remote Sensing of Environment*, **107**, pp. 276–286.

LOVELAND, T.R., REED, B.C., BROWN, J.F., OHLEN, D.O., ZHU, Z., YANG, L. and MERCHANT, J.W., 2000, Development of a global land cover characteristics database and IGBP DIScover from 1 km AVHRR data. *International Journal of Remote Sensing*, **21**, pp. 1303–1330.

LUCHT, W., SCHAAF, C.B. and STRAHLER, A.H., 2000, An algorithm for the retrieval of albedo from space using semiempirical BRDF models. *IEEE Transactions on Geosciences and Remote Sensing*, **38**, pp. 977–998.

JENSEN, J.R., 2005, *Introductory Digital Image Processing: A Remote Sensing Perspective*, 3rd edn (Upper Saddle River, NJ: Prentice Hall).

KIMES, D.S., HARRISON, P.R. and HARRISON, P.A., 1991, Learning class descriptions from a data base of spectral reflectance with multiple view angles. *IEEE Transactions on Geosciences and Remote Sensing*, **30**, pp. 315–325.

KREMER, R.G. and RUNNING, S.W., 1993, Community type differentiation using NOAA/AVHRR data within a sagebrush steppe ecosystem. *Remote Sensing of Environment*, **46**, pp. 311–318.

MARTONCHIK, J.V., PINTY, B. and VERSTRAETE, M.M., 2002, Note on: An improved model of surface BRDF-atmospheric coupled radiation. *IEEE Transactions on Geosciences and Remote Sensing*, **40**, pp. 1637–1639.

MULDAVIN, E., SHORE, G., TAUGHER, K. and MILNE, B., 1998, *A Vegetation Classification and Map for the Sevilleta National Wildlife Refuge, New Mexico*, Final Report to the New Mexico Natural Heritage Program and Sevilleta Long Term Ecological Research Program, (Albuquerque, NM: University of New Mexico).

MYNENI, R.B. and ASRAR, G., 1993, Radiative transfer in three-dimensional atmosphere-vegetation media. *Journal of Quantitative Spectroscopy and Radiative Transfer*, **49**, pp. 585–598.

NOLEN, B.A., DINTERMAN, P., KENNEDY, J.F., JONES, G. and AYARBE, L., 1999, New digitized databases. In *Proceedings of the 9th Annual Jornada Symposium*, Las Cruces, NM.

NOLIN, A.W., 2004, Towards the retrieval of forest cover density over snow from the Multi-angle Imaging SpectroRadiometer (MISR). *Hydrological Processes*, **18**, pp. 3623–3636.

RAHMAN, H. and DEDIEU, G., 1994, SMAC: a simplified method for the atmospheric correction of satellite measurements in the solar spectrum. *International Journal of Remote Sensing*, **15**, pp. 123–143.

RAHMAN, H., PINTY, B. and VERSTRAETE, M.M., 1993, Coupled surface-atmosphere reflectance (CSAR) model 2. Semiempirical surface model usable with NOAA Advanced Very High 93 Resolution Radiometer data. *Journal of Geophysical Research*, **98**, pp. 20791–20801.

RANGO, A., RITCHIE, J.C., KUSTAS, W.P., SCHMUGGE, T.J. and HAVSTAD, K.M., 1998, JORNEX: remote sensing to quantify long-term vegetation change and hydrological fluxes in an arid rangeland environment. In *Hydrology in a Changing Environment*, H. Wheater and C. Kirby (Eds) pp. 585–590 (London: John Wiley).

ROSS, J., 1981, *The Radiation Regime and Architecture of Plant Stands* (Boston, MA: W. Junk).

ROUJEAN, J.L., LEROY, M. and DESCHAMPS, P.Y., 1992, A bidirectional reflectance model of the Earth's surface for the correction of remote sensing data. *Journal of Geophysical Research*, **97**, pp. 20455–20468.

SANDMEIER, S. and DEERING, D.W., 1999, Structure analysis and classification of Boreal forests using airborne hyperspectral BRDF data from ASAS. *Remote Sensing of Environment*, **69**, pp. 281–295.

SARLE, W.S., 1997, Neural Network FAQ. Periodic posting to the Usenet newsgroup comp.ai.neural-nets (ftp://ftp.sas.com/pub/neural/FAQ.html).

SCHAAF, C.B., GAO, F., STRAHLER, A.H., LUCHT, W., LI, X., TSANG, T., STRUGNELL, N.C., ZHANG, X., JIN, Y., MULLER, J., LEWIS, P., BAMSLEY, M., HOBSON, P., DISNEY, M., ROBERTS, G., DUNDERDALE, M., DOLL, C., D'ENTREMONT, R.P., HU, B., LIANG, S., PRIVETTE, J.L. and ROY, D., 2002, First operational BRDF, albedo and nadir reflectance products from MODIS. *Remote Sensing of Environment*, **83**, pp. 135–148.

STRAHLER, A.H., LOGAN, T.L. and BRYANT, N.A., 1978, Improvement forest cover classification accuracy from Landsat by incorporating topographic information. In *Proceedings of the 12th International Symposium on Remote Sensing of the Environment*, pp. 927–942, (Ann Arbor, MI: Environmental Research Institute of Michigan).

SU, L., CHOPPING, M.J., RANGO, A., MARTONCHIK, J.V. and PETERS, D.P.C., 2007a, Support vector machines for recognition of semi-arid vegetation types using MISR multi-angle imagery. *Remote Sensing of Environment*, **107**, pp. 299–311.

SU, L., CHOPPING, M.J., RANGO, A., MARTONCHIK, J.V. and PETERS, D.P.C., 2007b, Differentiation of semi-arid vegetation types based on multi-angular observations from MISR and MODIS. *International Journal of Remote Sensing*, **28**, pp. 1419–1424.

VAPNIK, V., 1995, *The Nature of Statistical Learning Theory* (New York, NY: Springer-Verlag).

VERSTRAETE, M.M., PINTY, B. and DICKINSON, R.E., 1990, A physical model of the bidirectional reflectance of vegetation canopies. 1: Theory. *Journal of Geophysical Research*, **95**, pp. 11755–11765.

WANNER, W., LI, X. and STRAHLER, A.H., 1995, On the derivation of kernels for kernel-driven models of bidirectional reflectance. *Journal of Geophysical Research*, **100**, pp. 21077–21090.

WILKINSON, G.G., 2005, Results and implications of a study of fifteen years of satellite image classification experiments. *IEEE Transactions on Geoscience and Remote Sensing*, **43**, pp. 433–440.

XAVIER, A.S. and GALVÃO, L.S., 2005, View angle effects on the discrimination of selected Amazonian land cover types from a principal-component analysis of MISR spectra. *International Journal of Remote Sensing*, **26**, pp. 3797–3811.

ZHANG, Y., TIAN, Y., MYNENI, R.B., KNYAZIKHIN, Y. and WOODCOCK, C.E., 2002, Assessing the information content of multiangle satellite data for mapping biomes: I. Statistical analyses. *Remote Sensing of Environment*, **80**, pp. 418–434.